analytical chemistry

Article

pubs.acs.org/ac

Quantitative Profiling of Nanoscale Liposome Deformation by a Localized Surface Plasmon Resonance Sensor

Joshua A. Jackman,[†] Saziye Yorulmaz Avsar,[†] Abdul Rahim Ferhan,[†] Danlin Li,[†] Jae Hyeon Park,[†] Vladimir P. Zhdanov,[†,§] and Nam-Joon Cho*[,†,‡]

[†]School of Materials Science and Engineering and Centre for Biomimetic Sensor Science, Nanyang Technological University, 50 Nanyang Drive, 637553, Singapore

[‡]School of Chemical and Biomedical Engineering, Nanyang Technological University, 62 Nanyang Drive, 637459, Singapore

[§]Boreskov Institute of Catalysis, Russian Academy of Sciences, Novosibirsk 630090, Russia

ABSTRACT: Characterizing the shape of sub-100 nm, biological soft-matter particulates (e.g., liposomes and exosomes) adsorbed at a solid-liquid interface remains a challenging task. Here, we introduce a localized surface plasmon resonance (LSPR) sensing approach to quantitatively profile the deformation of nanoscale, fluid-phase 1,2-dioleoyl-*sn*-glycero-3-phosphocholine (DOPC) liposomes contacting a titanium dioxide substrate. Experimental and theoretical results validate that, due to its high sensitivity to the spatial proximity of phospholipid molecules near the sensor surface, the LSPR sensor can discriminate fine differences in the extent of ionic strength-modulated liposome deformation at both low and high surface coverages. By contrast, quartz crystal microbalance-dissipation (QCM-D) measurements performed with equivalent samples were qualitatively sensitive to liposome deformation only at saturation coverage. Control experiments with stiffer, gel-phase 1,2-dipalmitoyl-*sn*-glycero-3-phosphocholine (DPPC) liposomes verified that the LSPR measurement discrimination arises from the extent of liposome deformation, while the QCM-D measurements yield a more complex response that is also sensitive to the motion of adsorbed liposomes and coupled solvent along with lateral interactions between liposomes. Collectively, our findings demonstrate the unique measurement capabilities of LSPR sensors in the area of biological surface science, including competitive advantages for probing the shape properties of adsorbed, nanoscale biological particulates.

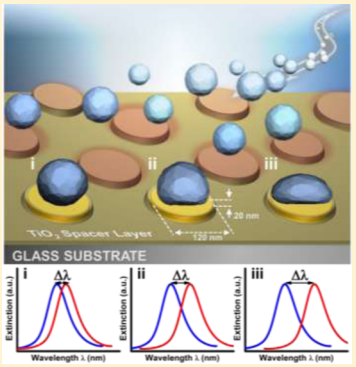

Characterizing the adsorption behavior of biological macromolecules (e.g., proteins[1]) and nanoscale particulates (e.g., liposomes,[2] exosomes,[3,4] and virions[5]) at solid−liquid interfaces has long motivated the development of highly surface-sensitive measurement techniques. From a biological perspective, the shape of adsorbed, soft-matter particulates can strongly influence membrane curvature sensing and other nanoscale phenomena.[6,7] Label-free measurement tools utilizing optical and acoustic transducers are among the most common experimental approaches in order to probe the mass and shape of such species.[8] Depending on the application, different types of sensor techniques have relative merits based on the underlying physical principles of the measurement response and corresponding sensitivity to different properties of the adsorbate. Historically, surface plasmon resonance (SPR) sensors based on the use of evanescent light were among the first and most successful approaches in this area.[9] However, the characteristic decay length of the SPR evanescent field (from 100 to 600 nm) is typically much longer than the size of adsorbed macromolecules and comparable or longer to the size of biological particulates. As a result, SPR sensors are optimal for determining the total mass uptake but provide scant information about the shape of adsorbates[10−13] (for recent advances in the use of this technique in general and its dual-wavelength version in particular for characterization of adsorbed exosomes, see refs 3 and 4). On the other hand, acoustic sensors such as the quartz crystal microbalance with dissipation (QCM-D) monitoring (with typical penetration length of 60−250 nm) provide detailed information about the hydrodynamically coupled mass and dynamical properties of adsorbed soft matter and it is sometimes possible to distinguish between the likely shapes of adsorbed species.[14,15] A classic example is its discrimination toward adsorbed phospholipid molecules in different membrane configurations.[14] However, interpretation of QCM-D data is complicated by numerous factors, including lack of direct correlation between the measurement response and surface coverage of adsorbate[16] as well as challenges to model the hydrodynamic properties of heterogeneous soft matter adlayers in the form of discrete particles.[17] While model-independent analysis has shown promise for studying adsorption of rigid particles,[18−20] it remains difficult to predict reliably the size and shape of adsorbed species in general.[21] Altogether, these challenges highlight the importance and largely unmet need of developing analytical strategies to directly probe the shape properties of adsorbed, nanoscale soft-matter particulates.

Received: July 4, 2016
Accepted: December 16, 2016
Published: December 16, 2016

DOI: 10.1021/acs.analchem.6b02532
Anal. Chem. 2017, 89, 1102−1109

To address this need, localized surface plasmon resonance (LSPR) sensors appear to be a promising solution. The LSPR sensing approach is based on excitation of the coherent oscillation of conduction band electrons in a metallic nanostructure by light with a resonant frequency that defines the maximum-extinction wavelength, λ_{max}.[22−24] Because such nanostructures have a tightly confined evanescent field[25] (typical decay length depends on the nanodisk size and is expected to be less than 20 nm as discussed in ref 37), λ_{max} is highly sensitive to changes in the local refractive index. This feature sets the basis for wide application of LSPR sensors in different areas.[26−30] In our context, we may mention previous studies reporting detection of conformational changes in a protein adlayer,[1] characterizing location-specific binding upon nanostructures[31] as well as tracking the kinetics of the rupture of adsorbed liposomes leading to formation of a supported lipid bilayer.[32,33] Moreover, there are ongoing advances to integrate arrays of nanoplasmonic structures on solid supports with thin dielectric coatings,[34] functionalized biomimetic interfaces,[35] topographically flat surfaces,[36] and optimized detection capabilities[37] in order to expand the scope of biosensing applications. Despite these advances, the application of LSPR sensors to investigate the shape properties of adsorbates at solid−liquid interfaces remains scarce. In the few existing studies, it has been shown that the λ_{max} shift is sensitive to the geometrical size and membrane phase state of liposomes adsorbed up to the critical coverage for their rupture.[38,39] It has also been possible to distinguish the enhanced interaction between liposomes and TiO_2 versus SiO_2 substrates.[40] Collectively, these results imply the strong potential of LSPR measurements to profile the deformation of adsorbed liposomes, which represent an ideal model adsorbate considering the comparable values of liposome size and the LSPR decay length. Indeed, the latter length is shorter than the liposome size, and accordingly the LSPR technique is expected to be particularly sensitive to the area just near the liposome-substrate contact region. However, LSPR studies of this category combined with detailed interpretation of the results at low and high surface coverages are lacking, and addressing this gap would be a significant advance to validate the potential of LSPR measurements for nanoscience characterization applications involving soft-matter adsorbates.

Herein, we report that the LSPR measurement technique can be used to quantitatively profile the extent of liposome deformation under different environmental conditions, obtained in this case by changing the ionic strength in solution. In particular, the ionic strength was varied by adjusting the NaCl concentration in the bulk solution. Experiments were conducted with liposomes in the gel-phase and fluid-phase membrane states. For fluid-phase liposomes with relatively low bending rigidity, the variation in ionic strength results in a positive or negative osmotic pressure across the liposomal bilayer and also influences the liposome-substrate interaction. In particular, positive osmotic pressures induce shape deformation of liposomes and strengthen the lipid-substrate interaction, while negative osmotic pressures inhibit shape deformation and weaken the liposome-substrate interaction.[41−43] In the case of positive osmotic pressures, the extent of shape deformation is determined by a compromise between reducing the volume of the liposome interior and increasing membrane bending. On the other hand, gel-phase liposomes with higher bending rigidity are appreciably less sensitive to ionic strength variations on the account of stiffer membranes.[44] In complement to these comprehensive experiments, we present a detailed theoretical treatment in order to validate our approach and conclusions.

MATERIALS AND METHODS

Liposome Preparation. Liposomes composed of 1,2-dioleoyl-*sn*-glycero-3-phosphocholine (DOPC) or 1,2-dipalmitoyl-*sn*-glycero-3-phosphocholine (DPPC) (Avanti Polar Lipids, Alabaster, AL) were prepared by the extrusion method. Dried lipid films were hydrated in aqueous buffer solution (10 mM Tris [pH 7.5] with 150 mM NaCl) at a lipid concentration of 5 mg/mL. After vortexing the sample, the liposomes were extruded through track-etched polycarbonate members with 50 nm diameter nominal pore sizes. For DPPC liposomes, the same extrusion procedure was followed but it was conducted at a higher temperature, above the DPPC gel-to-fluid phase transition temperature of 41 °C. Before extrusion, the hydrated DPPC lipid suspension was heated to 60 °C using a water bath and the extruder block was heated to 70 °C on a hot plate. The extruded liposomes were diluted in the appropriate buffer solution immediately before experiment. All aqueous solutions were prepared in Milli-Q-treated water with a minimum resistivity of 18.2 MΩ cm (Millipore, Billerica, MA).

Quartz Crystal Microbalance-Dissipation (QCM-D). Experiments were conducted with a Q-Sense E4 instrument (Biolin Scientific AB, Stockholm, Sweden). The sensor substrates had a fundamental frequency of 5 MHz and a sputter-coated, 50 nm thick layer of titanium (model no. QSX 310, Biolin Scientific AB). In all steps, a peristaltic pump (Reglo Digital, Ismatec, Glattbrugg, Switzerland) was used to inject liquid samples into the measurement chamber at a flow rate of 50 μL/min. The temperature in the measurement chamber was maintained at 25.0 ± 0.5 °C. The experimental data were collected at multiple odd overtones using the QSoft software program (Biolin Scientific AB), and the data were normalized according to the overtone number. All presented data were collected at the fifth overtone. Voigt-Voinova modeling was performed in the QTools software program (Biolin Scientific AB), and the effective parameters describing the viscoelastic properties of the adlayer were obtained by constraining the uniform effective density and viscosity of the bulk aqueous solution to be 1000 kg m^{-3} and 0.001 Pa s^{-1}, respectively.

Localized Surface Plasmon Resonance (LSPR). Ensemble-averaged LSPR measurements were performed in optical transmission mode by using an Insplorion XNano instrument (Insplorion AB, Gothenburg, Sweden), as previously described.[38] Data analysis was conducted with the Insplorer software package (Insplorion AB). The spectral resolution of the plasmon resonance, including the centroid position, is determined by high-order polynomial fitting. The sensor chips (Insplorion AB) consisted of a glass slide with deposited and well-separated gold nanodisks (surface coverage ∼8%). The sensor chip's surface was coated by a sputtered titanium dioxide film (thickness ∼10 nm), and the individual coated nanodisks had an average height and diameter of 20 and 120 nm, respectively. During experiment, liquid sample was continually introduced by a peristaltic pump (Reglo Digital, Ismatec) at a constant flow rate of 50 μL/min. For each experimental series, the measurement data were collected on a single sensor chip in order to avoid differences in surface sensitivity, and there is high reproducibility (±0.1 nm) in the final responses.

DOI: 10.1021/acs.analchem.6b02532
Anal. Chem. 2017, 89, 1102−1109

RESULTS AND DISCUSSION

Measurement Strategy. The concept of the LSPR measurement strategy is presented in Figure 1. The LSPR

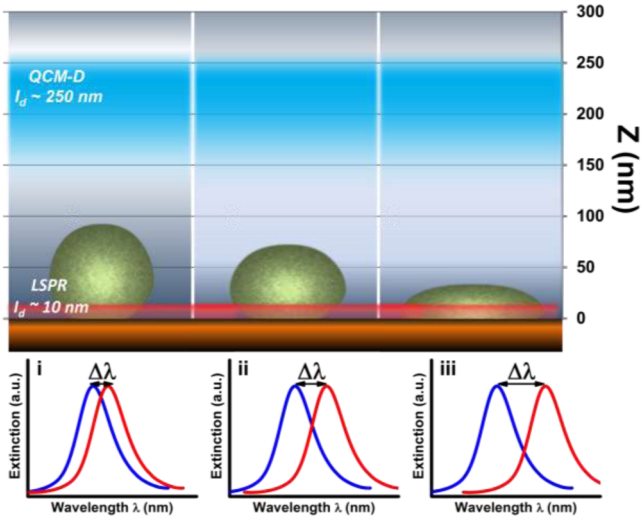

Figure 1. Schematic illustration of LSPR principle to measure deformation of adsorbed liposomes. The corona across the surface symbolizes the evanescent field and its decay length is around 10 nm. In actual experiments, the corona is confined to the near-vicinity of individual TiO_2-coated gold nanodisks on a glass surface. For comparison, the penetration depth of conventional QCM-D measurements is shown to be around 250 nm. Panels i–iii show examples of how the peak shift depends on the shape of the adsorbed liposome. The blue and red curves in the spectrograms correspond to before and after liposome addition, respectively. With increasing deformation of adsorbed liposomes, the corresponding peak shift ($\Delta\lambda$) becomes greater because the lipid mass is, on average, nearer to the sensor surface and hence more of the lipid mass is within the LSPR evanescent field.

sensing platform consists of an array of plasmonic gold nanodisks (~120 nm diameter and ~20 nm height) that are fabricated on a glass surface by hole-mask colloidal lithography, and the substrate is coated with a thin (~10 nm) TiO_2 dielectric layer. TiO_2 was chosen so that adsorbed liposomes do not rupture[45,46] and accordingly their state can be characterized at the onset of adsorption and at saturation as well. The sensor chip is configured in a flow-through microfluidic chamber that enables tracking the kinetics of liposome adsorption onto the surface with an ensemble-averaged measurement readout. The distance between nearest-neighbor disks was 500 nm in order to minimize disk-disk interactions. There is a single extinction peak (λ_{max} is around 760 nm), and the centroid position of this peak is evaluated as a function of time in order to measure the corresponding adsorption kinetics, with the $\Delta\lambda_{max}$ recorded relative to a baseline measurement in aqueous buffer solution (without liposome).[47]

When individual liposomes adsorb onto the substrate, there is a positive contribution to the $\Delta\lambda_{max}$ shift because phospholipids have a higher refractive index than aqueous buffer solution. As more liposomes adsorb onto the substrate, the recorded $\Delta\lambda_{max}$ shift further increases and, during the initial stages of liposome adsorption when the surface coverage of adsorbed liposomes remains low, the rate of change in the $\Delta\lambda_{max}$ shift has a linear slope because the adsorption rate of liposomes is limited by their diffusion in bulk solution. Under fixed experimental conditions (e.g., flow rate, liposome size, liposome concentration), the slope of the curve in this linear regime of the $\Delta\lambda_{max}$ shift varies according to the extent of deformation of adsorbed liposomes because the measurement response is greater when the phospholipids are, on average, closer to the sensor surface. As a result, a more-deformed liposome has a greater contribution to the $\Delta\lambda_{max}$ shift than a less-deformed liposome, and this difference is particularly pronounced at low surface coverages. As the number of adsorbed liposomes on the substrate increases, the packing density of adsorbed liposomes eventually reaches a saturation level, yielding a maximum $\Delta\lambda_{max}$ shift. While the rate of change in the $\Delta\lambda_{max}$ shift at low coverage depends primarily on the extent of liposome deformation only, the maximum $\Delta\lambda_{max}$ shift depends on both the total surface coverage and extent of deformation of the adsorbed liposomes. Therefore, the LSPR measurement approach provides multiple signals that can be utilized for measuring the extent of liposome deformation.

For comparison, we also conducted QCM-D measurements on a TiO_2-coated substrate. At present, QCM-D is one of the most common techniques to characterize liposome adsorption and was used here as a reference tool. Importantly, the probing volumes of the LSPR and QCM-D techniques vary and therefore the two measurement techniques yield different signals in response to liposome deformation. For more-deformed liposomes, it is expected that the LSPR signal will be greater than for less-deformed liposomes because the phospholipids are, on average, closer to the sensor surface as discussed above. By contrast, the QCM-D signals would be smaller for more-deformed vesicles because the effective thickness of the adlayer would decrease, the amount of coupled solvent would decrease as well, and the adsorbed liposomes would be more rigidly attached.

Effect of Ionic Strength on Liposome Adsorption. We begin by investigating the adsorption of fluid-phase, zwitterionic 1,2-dioleoyl-*sn*-glycero-3-phosphocholine (DOPC) liposomes onto the TiO_2 surface under varying ionic strength conditions. The liposomes were prepared by the extrusion method at 5 mg/mL lipid concentration and the average diameter, measured by dynamic light scattering, was around 75 nm. The aliquots were diluted accordingly to 0.05 mg/mL in the appropriate buffer solution immediately before the experiment. In all cases, the liposome interior contained 10 mM Tris buffer [pH 7.5] with 150 mM NaCl, while the bulk solution was 10 mM Tris buffer [pH 7.5] with varying NaCl salt concentration between 75 and 500 mM. Therefore, liposomes in 175 mM NaCl salt or greater ionic strength are subjected to positive osmotic pressure conditions while liposomes in 125 mM NaCl salt or lesser ionic strength are under negative osmotic pressure conditions. Liposomes in 150 mM NaCl salt are in isotonic conditions.

While zwitterionic liposomes under conventional ionic strength conditions are known to adsorb until saturation and remain intact on TiO_2,[45] their behavior under more extreme ionic strength and osmotic pressure conditions is less well understood. Therefore, we first investigated the kinetics of liposome adsorption onto a TiO_2-coated substrate by the conventional QCM-D technique (Figure 2). The corresponding resonance frequency and energy dissipation shifts (recorded at the fifth overtone) reflect the mass and viscoelastic properties of the solution and adsorbed liposome layer, respectively. In QCM-D measurements, when a soft-matter adsorbate such as a

DOI: 10.1021/acs.analchem.6b02532
Anal. Chem. 2017, 89, 1102–1109

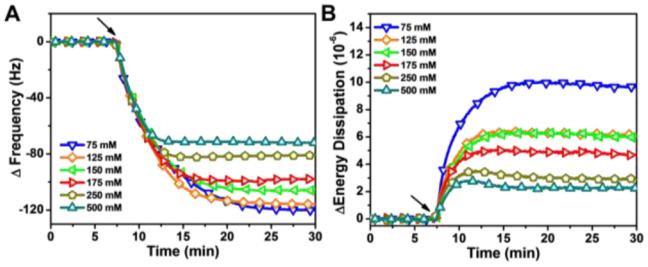

Figure 2. QCM-D measurement of fluid-phase DOPC liposome adsorption at different ionic strengths. Changes in (A) resonance frequency and (B) energy dissipation as a function of time. Liposomes were added at approximately t = 7 min (see arrows).

liposome attaches to the sensor surface, there is a decrease in the frequency shift and an increase in the energy dissipation shift. For these experiments, baseline signals in aqueous buffer solution were recorded before 0.05 mg/mL liposomes in equivalent solution were added at t = 7 min. In all cases, monotonic adsorption was observed, with significant decreases in resonance frequency and increases in energy dissipation. During the initial adsorption phase, the QCM-D frequency shift is independent of the ionic strength (Figure 2A). However, with increasing NaCl concentration, there was a clear trend in decreasing frequency shift at high coverages. At 75 mM NaCl, the frequency shift at saturation was around −122 Hz, while, at 500 mM NaCl, the final frequency shift was −73 Hz. Upon buffer washing, liposome adsorption was irreversible under the tested conditions except for the case of 75 mM NaCl (~80% reversible; at even lower ionic strengths, adsorption was negligible or fully reversible due to a weaker liposome-substrate interaction). The corresponding QCM-D energy dissipation shifts recorded at liposome saturation decreased with increasing salt concentration from 10×10^{-6} at 75 mM NaCl to 2×10^{-6} at 500 mM NaCl (Figure 2B). Taken together, the QCM-D data collected at the different salt concentrations indicate that, with increasing salt concentration, there are smaller resonance frequency and energy dissipation shifts, which possibly reflect greater deformation of adsorbed liposomes. The interpretation of these observations is, however, not simple because the effect of trapped water on both the QCM-D frequency and dissipation shifts may be appreciable and, even more subtly, may depend on the coverage even if the shape of attached particles remains the same (see, e.g., ref 21).

To more specifically address this point, we performed conventional QCM-D analysis based on the Voigt-Voinova model[48] implying that the adsorbed liposomes at saturation coverage can be treated as a homogeneous adlayer. On the basis of this approach, the effective thickness of the adlayer was extracted as a measure of liposome deformation (Table 1).

Table 1. Effective Thickness of Adsorbed DOPC Liposome Layers, l_{eff}, Predicted at Different External NaCl Salt Concentrations, c, by the Voigt-Voinova Model Analysis

c (mM)	l_{eff} (nm)
75	48.4
125	38.6
150	19.8
175	18.4
250	15.2
500	13.1

With increasing ionic strength, and accordingly an increase in positive osmotic pressure, the effective thickness of the adlayer decreased from 48 nm at 75 mM NaCl to 13 nm at 500 mM NaCl. While the trend in effective thickness agrees with the anticipated effect of osmotic pressure on liposome deformation, the values are inconsistent with adsorbed liposomes remaining intact. Such large deformations at high positive osmotic pressures would induce liposome rupture as explained below. The lack of liposome rupture under such conditions indicates that the extent of liposome deformation is less appreciable than that predicted by the corresponding effective film thickness, and this discrepancy underscores the challenge of applying QCM-D measurements to quantitatively probe liposome deformation.

As a control experiment, similar QCM-D measurements were also performed with gel-phase 1,2-dipalmitoyl-*sn*-glycero-3-phosphocholine (DPPC) liposomes of nearly equivalent size (~73 nm diameter) (Figure 3). These liposomes have a much

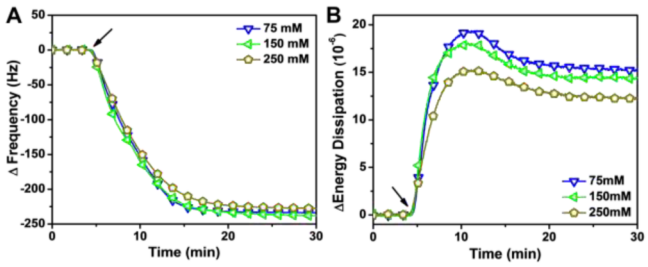

Figure 3. QCM-D measurement of gel-phase DPPC liposome adsorption at different ionic strengths. Changes in (A) resonance frequency and (B) energy dissipation as a function of time. Liposomes were added at approximately t = 5 min (see arrows).

higher membrane bending rigidity than fluid-phase liposomes and accordingly are less susceptible to osmotic pressure-induced shape deformation. Across the range of tested ionic strength conditions, DPPC liposome adsorption led to nearly equivalent frequency shifts around −225 Hz (Figure 3A). The observed frequency shifts indicate that ionic strength does not have a strong effect on the extent of gel-phase liposome deformation. However, at the same time, the kinetic curves of the dissipation shifts typically exhibited more complex, overshoot behavior indicating some kind of structural rearrangement, along with a large variation in the final dissipation shifts between 12 and 16 × 10^{-6} (Figure 3B). One likely reason for this variation in dissipation shifts is that, at low surface coverage, the adsorbed DPPC liposomes experience "rocking and rolling" motion across the surface.[19] Such cases have been previously reported by Reviakine et al. for sufficiently stiff, adsorbed liposomes whereas less stiff liposomes do not exhibit such behavior, as seen in the DOPC liposome case above.[19] This difference is also reasonable considering that less stiff liposomes have a greater liposome-surface contact area for the same equivalent liposome-substrate interaction energy and hence are less mobile on the substrate.[49] On the other hand, at higher surface coverages for the DPPC liposome case, the lateral interactions between adsorbed liposomes prevent this type of motion, effectively reducing dissipation in the thin film.

Despite the much larger frequency shifts for the adsorbed DPPC liposomes, the corresponding Voigt-Voinova modeling results indicate that the effective thickness of the adsorbed liposome layer is around 43 nm diameter in all cases. This value

DOI: 10.1021/acs.analchem.6b02532
Anal. Chem. 2017, 89, 1102−1109

is similar to the effective thickness of the adsorbed DOPC liposome layer for the 75 mM NaCl case for which deformation was expected to be minimal. However, considering that the adsorbed DPPC liposomes exhibit gel-phase membrane character with a high bending modulus, the results support that the viscoelastic model is insufficient to capture quantitative aspects of liposome deformation (~73 nm diameter in bulk solution versus ~43 nm height of the adsorbed liposome layer). In particular, the QCM-D measurements are highly sensitive to the surface coverage of adsorbed particles as well as hydrodynamics around the adsorbed particles. Therefore, while the QCM-D measurements indicate that the adsorbed liposomes remain intact and validate the experimental model system for evaluating the LSPR measurement capabilities, the results also reveal the challenges of probing liposome deformation, even on a relative scale, with this conventional approach.

Quantitative Evaluation of Liposome Deformation. In order to further probe liposome deformation in a more direct way, we therefore employed the LSPR technique utilizing an array of TiO_2-coated gold nanodisks deposited on a glass substrate (Figure 4). An identical series of fluid-phase, DOPC

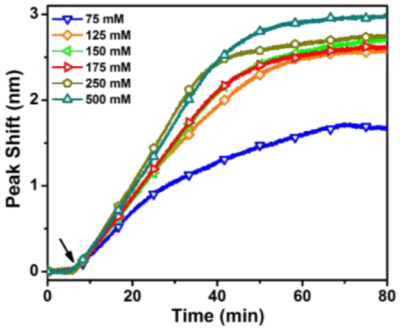

Figure 4. LSPR measurement of fluid-phase DOPC liposome adsorption as a function of time at different ionic strengths. Liposomes were added at approximately t = 7 min (see arrow).

liposome adsorption experiments was conducted as described above in order to follow the peak shift which occurs due to changes in the local refractive index around the nanodisk surface. After establishing a baseline signal in aqueous buffer solution, 0.05 mg/mL liposomes in equivalent solution were added at t = 7 min leading to a positive peak shift in all cases. With increasing ionic strength, the final peak shift was larger ranging from 1.6 nm at 75 mM NaCl to 2.9 nm at 500 mM NaCl. The variations in the final peak shifts were more appreciable at low ionic strength, while the peak shifts began to nearly converge at high ionic strength.

To determine the extent of liposome deformation, we focus on analyzing the initial phase of the adsorption kinetics as well as saturation. Because of their relatively large size, the diffusion of liposomes in solution is slow and their uptake is controlled by diffusion almost up to saturation.[50] Under our flow conditions, this means that the initial uptake is proportional to $D^{2/3}$ t, where t is time and D is the diffusion coefficient.[50] Hence, for liposomes of equivalent size, the rate of change in the LSPR signal for liposome adsorption at low surface coverage is controlled by the diffusion flux of liposomes onto the TiO_2 surface, and this value is influenced by the flow rate, liposome number concentration, and bulk diffusion coefficient, all of which are fixed in these experiments. An additional contribution to the rate of change in the LSPR signal comes from the deformation of individual adsorbed liposomes, reflecting the small probing volume of the LSPR sensor and its sensitivity to the proximity of phospholipids near the sensor surface. Assuming that the diffusion flux is equivalent across the tested ionic strength conditions, we can interpret that variations in the rate of change in the LSPR signal arise from differences in the extent of liposome deformation. Indeed, this initial rate is 0.049 nm/min for the 75 mM case versus 0.063 nm/min for the 150 mM case and 0.079 nm/min for the 250 mM case. Hence, with increasing ionic strength, there is a general trend toward greater initial rates of change in the LSPR signal.

To scrutinize the latter dependence, we use a model describing the mutual light-induced interaction between gold nanodisk sensors and deformed liposomes[38,39] (for its validation by 3D finite difference time-domain simulations, see ref 40) in terms of two dimensionless parameters. These parameters provide an indication of how liposome deformation influences the LSPR signal response for adsorbed liposomes when the surface coverage is low and at saturation. The first parameter, P_1, is defined as the ratio of the LSPR wavelength shifts for adsorbed liposomes in the deformed and non-deformed states provided the liposome surface concentration is low and the same irrespective of the extent of deformation (Figure 5). The latter one, P_2, is a similar ratio that is calculated

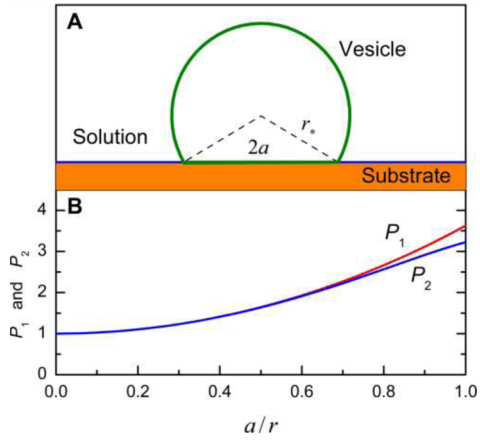

Figure 5. Effect of deformation of adsorbed liposomes on the LSPR signal. (A) A deformed liposome is represented as a truncated sphere with radius r_* ($r_* \geq r$). (B) Parameters P_1 and P_2 as a function of a/r for r = 38 nm and R_* = 74 nm (according to eqs 10 and 13 from ref 39; for validation of the value of the effective radius, R_*, of gold nanodisks, see ref 40).

provided liposomes are at saturation in the close-packed state. The governing parameter is considered to be $p \equiv a/r$, where a is the radius of the liposome-substrate contact area and r is the radius of a nondeformed liposome. Formally, p may be in the range from 0 up to $2^{1/2}$, but at $p > 1$ the deformation is strong and such liposomes are expected to rupture; hence, $p \leq 1$ is a sufficient range for the present analysis.

Assuming that DOPC liposome deformation at low ionic strength (75 mM) is nearly negligible, i.e., $a/r = 0$ and $P_1 = 1$ (because the liposomes are weakly bound and nearly ready to desorb in this case), we obtain that this shift corresponds to $a/r \approx 0.5$ and $P_1 = 1.61$ for adsorbed liposomes under a high ionic strength (250 mM). Under such conditions, the effect of ionic strength on the saturation uptake is expected to follow a similar trend (because P_2 is close to P_1), and the increase of the LSPR

DOI: 10.1021/acs.analchem.6b02532
Anal. Chem. 2017, 89, 1102−1109

signal should be of the same scale as that during the initial phase. This prediction is in agreement with our observations obtained by the LSPR measurements, with $a/r \approx 0.5$ and $P_2 = 1.64$ for adsorbed liposomes under a high ionic strength (250 mM). As such, the experimentally determined P_1 and P_2 values show good agreement and support the validity of the LSPR measurement approach.

We have also estimated the lipid bilayer bending constant for the small liposomes (~75 nm diameter) used in this study, for which the membrane curvature is appreciable. Under such circumstances, the bending constant may depend on curvature (i.e., it should be considered as an effective constant), and its value may be much greater than that conventionally measured in the low-curvature limit. To estimate the effective bending constant, we consider that, in the adsorbed state, the shape of a liposome depends on the adhesive energy, w, bending constant, κ, and osmotic pressure $k_BT\Delta c$. According to phenomenological analysis,[51] the effect of pressure is appreciable provided

$$k_BT\Delta cR^3/\kappa > 5 \tag{1}$$

where R is the liposome radius in the situation when its shape is spherical. Assuming the changes of the liposome shape to be related in our case with osmotic pressure and taking into account that the initial NaCl concentration is 150 mM while the external concentration is up to 500 mM, we use 200 mM as a scale of Δc and obtain that the scale of the bending constant is $\kappa \cong k_B\ T\Delta cR^3/5 \cong 1300k_BT$ (provided R = 38 nm). This value is appreciably higher than that, $\kappa \cong 25k_BT$, often used in the theoretical literature.[52] The conventionally measured values of κ are, however, reported to be in a wide range (see, e.g., refs 19, 53, and references therein) and the maximal values, $\sim 600k_BT$, are comparable with our estimate. In fact, the maximum value, measured in J, was 10^{-19} J (ref 19). Recently, Takechi-Haraya et al. explicitly showed by using atomic force microscopy (AFM) that the values of κ for small liposomes are on this scale and the maximum value, 2×10^{-19} J (see, e.g., Figure 5 in ref 44), is even higher.[44] As such, multiple independent results are in line with our estimates. Our previous analysis[54] of peptide-induced rupture of small liposomes was also indicative of a higher value for the bending constant of smaller liposomes. Along this line, we can add that with increasing osmotic pressure the bending energy rapidly increases (this is evident from the increase of the initial slope of the LSPR signal (cf. Figure 4)), and accordingly an additional increment of pressure is expected to result in a smaller contribution to liposome deformation. This explains why the LSPR peak shifts begin to nearly converge at high ionic strength.

The dependence of the initial slope of the LSPR signal on ionic strength (cf. Figure 3) may also be related to the effect of osmotic pressure on the liposome shape in solution. This may result in changes in the liposome shape and related changes in D and uptake. In this context, it is of interest to evaluate the expected time scale of equalization of osmotic pressure and the scale of the effect of osmotic pressure on D. Equalization of this pressure, expressed as the difference of ion concentrations, Δc, inside a liposome with respect to the bulk solution is limited by lowest permeability of the ions, Na^+ and Cl^-, inducing this pressure. This process is described as

$$V\frac{d\Delta c}{dt} = -PS\Delta c \tag{2}$$

where P is the permeability coefficient, and V and S are the volume and surface area of a liposome. If the liposome shape is close to spherical, then $V \cong 4\pi R^3/3$ and $S \cong 4\pi R^2$, and accordingly the time scale characterizing the process can be represented as

$$\frac{1}{\tau} = \frac{PS}{V} \cong \frac{3P}{R} \tag{3}$$

Detailed experimental measurements of the coefficients of permeability of lipid bilayers have been performed for potassium ions (see ref 55 and references therein). The corresponding published values are in the range from 10^{-13} and 10^{-9} cm/s, depending on technique and type of lipid. For sodium ions, the permeability coefficients were found to be somewhat smaller by a factor down to 1 order of magnitude.[56] The reported values for the permeability coefficient of chloride ions in liposomes are higher, from 10^{-8} cm/s to 10^{-11} cm/s.[57] Thus, the equalization of osmotic pressure appears in our case to be controlled by sodium ions, and the corresponding value of P is expected to be lower than 10^{-13} to 10^{-9}. Using these values and R = 38 nm, we obtain $\tau > 10^3$–10^7 s. On average, this time scale is much longer than that characterizing our measurements, and equalization of osmotic pressure is therefore unlikely even at the lower limit of the time scale.

Concerning liposome diffusion in solution, we note that according to hydrodynamics the value of D depends on the liposome shape. Because of the positive osmotic pressure at high ionic strengths, the volume of a liposome may be reduced, and its shape may be changed from ellipsoidal to circular biconcave.[58,59] To estimate the role of this factor, the liposome shape can be approximated as an ellipsoid of revolution characterized by one minor semiaxis length, a, and two equal major semiaxis lengths, $b > a$. For this geometry, the diffusion coefficient can be represented as[60]

$$D = \frac{k_BT}{6\pi\eta a}\frac{\mathrm{arctg}(\rho^2 - 1)^{1/2}}{(\rho^2 - 1)^{1/2}} \tag{4}$$

where η is the viscosity coefficient, and $\rho \equiv b/a$ is the aspect ratio. For a spherical liposome with $a = b \equiv a_0$, this expression yields the well-known result, $D = D_0 \equiv \frac{k_BT}{6\pi\eta a_0}$. For $a \neq b$, eq 4 should be used provided the liposome area is conserved, i.e., is equal to $4\pi a_0^2$. In the extreme case, the effect of osmotic pressure on diffusion will be maximum if the pressure is high and a liposome is fully flattened, i.e., $a \to 0$ and $b \cong 2^{1/2}a_0$. In this limit, eq 4 yields $D = (\pi/2^{3/2})D_0$, i.e., the diffusion coefficient increase by a factor of $\pi/2^{3/2} = 1.11$ or 11%. In the present experiments, the extent of deformation is relatively modest (i.e., liposomes are not fully flattened) and a more realistic estimate of the maximum increase of D is about half of this value, i.e., ≅5–7%. The related increase in the uptake is low (smaller or about 3–5%) and can be neglected. Thus, the dependence of the initial slope of the LSPR signal on ionic strength is related primarily to the dependence of the LSPR signal on the shape of adsorbed liposomes. That is, during the initial adsorption of liposomes at low coverage, differences in the slope of the LSPR signal are attributed to variations in the deformation of individual, adsorbed liposomes on the TiO_2 substrate.

As an additional experimental control, we conducted similar LSPR measurements using gel-phase DPPC liposomes under varying ionic strength conditions. As DPPC liposomes have

DOI: 10.1021/acs.analchem.6b02532
Anal. Chem. 2017, 89, 1102–1109

higher membrane bending rigidities, they are less susceptible to osmotic pressure-induced deformation and hence these experiments provide verification in order to clarify if the osmotic pressure-induced variations in DOPC liposome adsorption are in fact due to high sensitivity to the extent of liposome deformation. In marked contrast to the fluid-phase DOPC liposome case, the LSPR-tracked adsorption kinetics of the DPPC liposomes were nearly identical under all tested ionic strength conditions (Figure 6). The initial rate of change in the

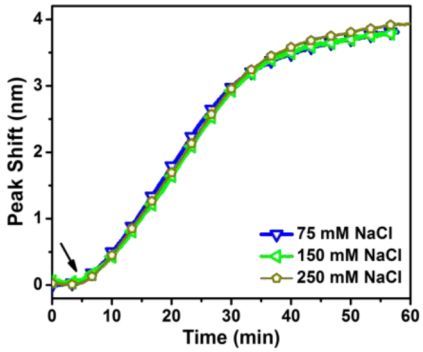

Figure 6. LSPR measurement of gel-phase DPPC liposome adsorption as a function of time at different ionic strengths. Liposomes were added at approximately t = 5 min (see arrow).

LSPR signal had similar slopes in all DPPC liposome cases while the final peak shifts were quite similar, and there was only a slight increase (~0.1 nm) at 250 mM NaCl which indicated very minor additional deformation due to positive osmotic pressure. As such, the similar LSPR measurement responses for DPPC liposome adsorption verify that the LSPR measurement technique is tracking variations in the osmotic pressure-induced deformation of fluid-phase DOPC liposomes. Hence, in direct comparison, the LSPR measurement responses strongly depended on ionic strength for fluid-phase (DOPC) liposomes in which case liposome deformation is tunable, whereas there was no dependence for gel-phase (DPPC) liposomes which are appreciably stiffer and more resistant to ion-induced shape deformation. On a separate note, the LSPR peak shifts for DPPC liposome adlayers were ~30% greater than for DOPC liposome adlayers and, considering that the liposome sizes were nearly equivalent, this difference is most probably explained by the fact that the packing area per phospholipid area in gel-phase DPPC liposomes is appreciably greater than in fluid-phase DOPC liposomes. As such, DPPC liposomes have a greater areal density of phospholipids in each liposome and therefore contribute to a larger measurement response, highlighting additional features of this LSPR sensing approach that can be further explored in future studies.

In summary, our results demonstrate that the LSPR measurement approach is capable of quantitatively profiling the extent of liposome deformation, with consistent interpretation of liposome deformation across both low and high surface coverages and for different phase states. By contrast, interpreting the results of conventional QCM-D measurements is complicated by the dependence on surface coverage, lateral interactions between adsorbed liposomes, coupled solvent, and the dissipative motion of stiff, adsorbed liposomes. Likewise, other surface-sensitive measurement techniques also have similar challenges for detecting and quantifying liposome deformation and related phenomena. As mentioned above, SPR is only faintly sensitive, if at all, to the shape of nanoscale adsorbates due to the mismatch between the length scales of the adsorbate and the decay of the evanescent field. Another possible measurement solution is AFM (see, e.g., refs 44 and 61). Although the AFM technique allows one to estimate the membrane bending constant in adsorbed liposomes,[44] its utility is limited to characterizing adsorbed particles at low coverage in a postadsorption state, the tip may deform liposomes or even result in their rupture, and such measurements are technically challenging. Taking into account all these points, the findings in this work demonstrate the unique merits of LSPR sensors for highly sensitive, nonperturbative characterization of the conformational and shape properties of nanoscale soft-matter adsorbates at solid-liquid interfaces. Such information is important from various fundamental and applied perspectives, especially in the context of nanoarchitectonics through which materials are viewed through the lens of dynamic interactions and functionalities[62] and components such as thermally tunable plasmonic materials open new sensing opportunities.[63] Indeed, the combination of experimental and theoretical treatments presented here motivates further exploration of LSPR sensors for nanoscience applications involving macromolecular and soft-matter adsorption processes.

AUTHOR INFORMATION

Corresponding Author

*E-mail: njcho@ntu.edu.sg.

ORCID

Nam-Joon Cho: 0000-0002-8692-8955

Notes

The authors declare no competing financial interest.

ACKNOWLEDGMENTS

The authors wish to acknowledge support from the National Research Foundation (Grant NRF2015NRF-POC001-019). V.P.Zh. is a recipient of the Tan Chin Tuan Exchange Fellowship at Nanyang Technological University.

REFERENCES

(1) Hall, W. P.; Modica, J.; Anker, J.; Lin, Y.; Mrksich, M.; Van Duyne, R. P. *Nano Lett.* **2011**, *11*, 1098−1105.
(2) Andrecka, J.; Spillane, K. M.; Ortega-Arroyo, J.; Kukura, P. *ACS Nano* **2013**, *7*, 10662−10670.
(3) Rupert, D. b. L.; Lässer, C.; Eldh, M.; Block, S.; Zhdanov, V. P.; Lotvall, J. O.; Bally, M.; Höök, F. *Anal. Chem.* **2014**, *86*, 5929−5936.
(4) Rupert, D. L.; Shelke, G. V.; Emilsson, G.; Claudio, V.; Block, S.; Lässer, C.; Dahlin, A.; Lötvall, J. O.; Bally, M.; Zhdanov, V. P.; Höök, F. *Anal. Chem.* **2016**, *88*, 9980−9988.
(5) Kukura, P.; Ewers, H.; Müller, C.; Renn, A.; Helenius, A.; Sandoghdar, V. *Nat. Methods* **2009**, *6*, 923−927.
(6) Hatzakis, N. S.; Bhatia, V. K.; Larsen, J.; Madsen, K. L.; Bolinger, P.-Y.; Kunding, A. H.; Castillo, J.; Gether, U.; Hedegård, P.; Stamou, D. *Nat. Chem. Biol.* **2009**, *5*, 835−841.
(7) Tabaei, S. R.; Rabe, M.; Zhdanov, V. P.; Cho, N.-J.; Höök, F. *Nano Lett.* **2012**, *12*, 5719−5725.
(8) Mashaghi, A.; Mashaghi, S.; Reviakine, I.; Heeren, R. M.; Sandoghdar, V.; Bonn, M. *Chem. Soc. Rev.* **2014**, *43*, 887−900.
(9) Homola, J. *Chem. Rev.* **2008**, *108*, 462−493.
(10) Reimhult, E.; Larsson, C.; Kasemo, B.; Höök, F. *Anal. Chem.* **2004**, *76*, 7211−7220.
(11) Reimhult, E.; Zäch, M.; Höök, F.; Kasemo, B. *Langmuir* **2006**, *22*, 3313−3319.
(12) Fang, J.; Wang, P.; Du, X.; Zhu, D.-M. *J. Phys. Chem. C* **2009**, *113*, 16121−16127.

DOI: 10.1021/acs.analchem.6b02532
Anal. Chem. 2017, 89, 1102−1109

(13) Fang, J.; Ren, C.; Zhu, T.; Wang, K.; Jiang, Z.; Ma, Y. *Analyst* **2015**, *140*, 1323−1336.
(14) Keller, C. A.; Kasemo, B. *Biophys. J.* **1998**, *75*, 1397−1402.
(15) Cho, N.-J.; Frank, C. W.; Kasemo, B.; Höök, F. *Nat. Protoc.* **2010**, *5*, 1096−1106.
(16) Reviakine, I.; Rossetti, F. F.; Morozov, A. N.; Textor, M. *J. Chem. Phys.* **2005**, *122*, 204711.
(17) Reviakine, I.; Johannsmann, D.; Richter, R. P. *Anal. Chem.* **2011**, *83*, 8838−8848.
(18) Tellechea, E.; Johannsmann, D.; Steinmetz, N. F.; Richter, R. P.; Reviakine, I. *Langmuir* **2009**, *25*, 5177−5184.
(19) Reviakine, I.; Gallego, M.; Johannsmann, D.; Tellechea, E. *J. Chem. Phys.* **2012**, *136*, 084702.
(20) Olsson, A. L.; Quevedo, I. R.; He, D.; Basnet, M.; Tufenkji, N. *ACS Nano* **2013**, *7*, 7833−7843.
(21) Grunewald, C.; Schmudde, M.; Noufele, C. N.; Graf, C.; Risse, T. *Anal. Chem.* **2015**, *87*, 10642−10649.
(22) Willets, K. A.; Van Duyne, R. P. *Annu. Rev. Phys. Chem.* **2007**, *58*, 267−297.
(23) Anker, J. N.; Hall, W. P.; Lyandres, O.; Shah, N. C.; Zhao, J.; Van Duyne, R. P. *Nat. Mater.* **2008**, *7*, 442−453.
(24) Mayer, K. M.; Hafner, J. H. *Chem. Rev.* **2011**, *111*, 3828−3857.
(25) Bertsch, G. F.; Broglia, R. A. *Oscillations in Finite Quantum Systems*; Cambridge University Press: Cambridge, England, 1994.
(26) Halas, N. J. *Nano Lett.* **2010**, *10*, 3816−3822.
(27) Larsson, E. M.; Edvardsson, M. E.; Langhammer, C.; Zorić, I.; Kasemo, B. *Rev. Sci. Instrum.* **2009**, *80*, 125105.
(28) Langhammer, C.; Larsson, E. M. *ACS Catal.* **2012**, *2*, 2036−2045.
(29) Dahlin, A. B.; Wittenberg, N. J.; Höök, F.; Oh, S.-H. *Nanophotonics* **2013**, *2*, 83−101.
(30) Estevez, M.-C.; Otte, M. A.; Sepulveda, B.; Lechuga, L. M. *Anal. Chim. Acta* **2014**, *806*, 55−73.
(31) Kumar, K.; Dahlin, A. B.; Sannomiya, T.; Kaufmann, S.; Isa, L.; Reimhult, E. *Nano Lett.* **2013**, *13*, 6122−6129.
(32) Jonsson, M. P.; Jönsson, P.; Dahlin, A. B.; Höök, F. *Nano Lett.* **2007**, *7*, 3462−3468.
(33) Jonsson, M. P.; Jonsson, P.; Höök, F. *Anal. Chem.* **2008**, *80*, 7988−7995.
(34) Langhammer, C.; Larsson, E. M.; Kasemo, B.; Zoric, I. *Nano Lett.* **2010**, *10*, 3529−3538.
(35) Galush, W. J.; Shelby, S. A.; Mulvihill, M. J.; Tao, A.; Yang, P.; Groves, J. T. *Nano Lett.* **2009**, *9*, 2077−2082.
(36) Jose, J.; Jordan, L. R.; Johnson, T. W.; Lee, S. H.; Wittenberg, N. J.; Oh, S. H. *Adv. Funct. Mater.* **2013**, *23*, 2812−2820.
(37) Mazzotta, F.; Johnson, T. W.; Dahlin, A. B.; Shaver, J.; Oh, S.-H.; Höök, F. *ACS Photonics* **2015**, *2*, 256−262.
(38) Jackman, J. A.; Zhdanov, V. P.; Cho, N.-J. *Langmuir* **2014**, *30*, 9494−9503.
(39) Oh, E.; Jackman, J. A.; Yorulmaz, S.; Zhdanov, V. P.; Lee, H.; Cho, N.-J. *Langmuir* **2015**, *31*, 771−781.
(40) Jackman, J. A.; Špačková, B.; Linardy, E.; Kim, M. C.; Yoon, B. K.; Homola, J.; Cho, N.-J. *Chem. Commun.* **2016**, *52*, 76−79.
(41) Hain, N.; Gallego, M.; Reviakine, I. *Langmuir* **2013**, *29*, 2282−2288.
(42) Zhu, T.; Jiang, Z.; Nurlybaeva, E. M. R.; Sheng, J.; Ma, Y. *Langmuir* **2013**, *29*, 6377−6385.
(43) Jackman, J. A.; Choi, J.-H.; Zhdanov, V. P.; Cho, N.-J. *Langmuir* **2013**, *29*, 11375−11384.
(44) Takechi-Haraya, Y.; Sakai-Kato, K.; Abe, Y.; Kawanishi, T.; Okuda, H.; Goda, Y. *Langmuir* **2016**, *32*, 6074−6082.
(45) Reimhult, E.; Höök, F.; Kasemo, B. *Langmuir* **2003**, *19*, 1681−1691.
(46) Jackman, J. A.; Zan, G. H.; Zhao, Z.; Cho, N.-J. *Langmuir* **2014**, *30*, 5368−5372.
(47) Dahlin, A. B.; Tegenfeldt, J. O.; Höök, F. *Anal. Chem.* **2006**, *78*, 4416−4423.
(48) Voinova, M.; Jonson, M.; Kasemo, B. *Biosens. Bioelectron.* **2002**, *17*, 835−841.
(49) Klacar, S.; Dimitrievski, K.; Kasemo, B. *J. Phys. Chem. B* **2009**, *113*, 5681−5685.
(50) Zhdanov, V. P.; Keller, C. A.; Glasmästar, K.; Kasemo, B. *J. Chem. Phys.* **2000**, *112*, 900−909.
(51) Seifert, U.; Lipowsky, R. *Phys. Rev. A: At., Mol., Opt. Phys.* **1990**, *42*, 4768.
(52) Smith, A.-S.; Sackmann, E.; Seifert, U. *Phys. Rev. Lett.* **2004**, *92*, 208101.
(53) Spyratou, E.; Cunaj, E.; Tsigaridas, G.; Mourelatou, E. A.; Demetzos, C.; Serafetinides, A. A.; Makropoulou, M. *J. Liposome Res.* **2015**, *25*, 202−210.
(54) Jackman, J. A.; Zan, G. H.; Zhdanov, V. P.; Cho, N.-J. *J. Phys. Chem. B* **2013**, *117*, 16117−16128.
(55) Paula, S.; Volkov, A.; Van Hoek, A.; Haines, T.; Deamer, D. W. *Biophys. J.* **1996**, *70*, 339.
(56) Papahadjopoulos, D. *Biochim. Biophys. Acta, Biomembr.* **1971**, *241*, 254−259.
(57) Paula, S.; Volkov, A.; Deamer, D. *Biophys. J.* **1998**, *74*, 319−327.
(58) Liu, Q.-H.; Haijun, Z.; Liu, J.-X.; Zhong-Can, O.-Y. *Phys. Rev. E: Stat. Phys., Plasmas, Fluids, Relat. Interdiscip. Top.* **1999**, *60*, 3227.
(59) Tu, Z.; Ou-Yang, Z. *Adv. Colloid Interface Sci.* **2014**, *208*, 66−75.
(60) Perrin, F. *J. Phys. Radium* **1936**, *7*, 11.
(61) Dimitrievski, K.; Zäch, M.; Zhdanov, V. P.; Kasemo, B. *Colloids Surf., B* **2006**, *47*, 115−125.
(62) Ariga, K.; Li, J.; Fei, J.; Ji, Q.; Hill, J. P. *Adv. Mater.* **2016**, *28*, 1251−1286.
(63) Lewandowski, W.; Fruhnert, M.; Mieczkowski, J.; Rockstuhl, C.; Górecka, E. *Nat. Commun.* **2015**, *6*, 6590.

DOI: 10.1021/acs.analchem.6b02532
Anal. Chem. 2017, 89, 1102−1109